PHOTONICS Research

2.8 μm all-fiber Q-switched and mode-locked lasers with black phosphorus

Zhipeng Qin, Guoqiang Xie,* Jingui Ma, Peng Yuan, and Liejia Qian

Key Laboratory for Laser Plasmas (Ministry of Education), Collaborative Innovation Center of IFSA (CICIFSA), School of Physics and Astronomy, Shanghai Jiao Tong University, Shanghai 200240, China
**Corresponding author: xiegq@sjtu.edu.cn*

Received 3 August 2018; revised 2 September 2018; accepted 2 September 2018; posted 5 September 2018 (Doc. ID 341246); published 18 October 2018

In past years, rare-earth-doped fluoride fiber lasers (FFLs) have developed rapidly in the mid-infrared (mid-IR) region. However, due to the lack of fiber optic devices and challenge of fluoride fiber splicing, most mid-IR FFLs have been demonstrated with free-space optic elements, limiting the advantages of all-fiber lasers for flexible delivery, stability, and compactness. Here, we report, to the best of our knowledge, the first pulsed all-fiber FFL in the mid-IR region. By taking advantage of the integration of black phosphorus flake, stable *Q*-switched and mode-locked pulses were obtained at 2.8 μm wavelength. We believe that this all-fiber design will promote the application of pulsed FFL in the mid-IR region. © 2018 Chinese Laser Press

https://doi.org/10.1364/PRJ.6.001074

1. INTRODUCTION

Mid-infrared (mid-IR) coherent sources are in great demand for a wide range of applications in spectroscopy, defense, trace gas sensing, and tissue imaging [1–4]. With the advances in fluoride fiber fabrication and deep understanding of radiation dynamics of rare-earth-doped fluoride fibers [5–8], high-efficiency and high-power fluoride fiber lasers (FFLs) have developed rapidly over recent years and become an important access to the mid-IR coherent source. However, fluoride glass has, compared to fused silica glass, worse mechanical properties, a lower glass transition temperature ($T_g \approx 265$°C), a larger thermal expansion coefficient (200×10^{-7} K^{-1}), and a lower thermal diffusivity (2.4×10^{-3} cm^2/s) [9], making it challenging to splice fluoride fibers and to develop fiber optic devices such as pump couplers, fiber optic isolators, and polarization controllers. Therefore, most FFLs have been built with free-space optic elements that limit the advantages of all-fiber lasers for flexible delivery, stability, and compactness.

Up to now, only continuous-wave (CW) all-fiber FFLs have been reported, which have been enabled by a pair of fiber Bragg gratings [10,11]. It has been shown that all-fiber FFL is superior to free-space FFL in output power stability [11,12]. Great efforts have been made to develop other fluoride-fiber-based integratable optic devices. Recently, a fluoride-fiber-based pump coupler has been fabricated, and CW output power of 15 W has been generated in a multimode double-clad Er:ZBLAN fiber laser [13]. For fluoride fiber splicing, a narrow working temperature range of 300–350°C is required. Fluoride fiber can be effectively heated by a CO_2 laser due to its strong absorption at 10.6 μm, and the generated heat can be controlled by the launched pump power. Heated by a CO_2 laser, fluoride-to-fluoride fiber splicing has been realized [13]. As for silica-to-fluoride fiber spicing, the silica fiber can be heated by an electrode-based fusion splicer, and then two fibers are spliced immediately [14].

For achieving pulsed operation, a suitable saturable absorber (SA) is generally necessary in the FFL. In past years, the widely used SAs in the mid-IR region include a commercial semiconductor saturable absorber mirror (SESAM) and two-dimensional (2D) materials such as graphene, topological insulators (TIs), transition metal dichalcogenides (TMDs), and black phosphorus (BP) [15–31]. Compared to SESAM, 2D SAs can be easily fabricated and integrated into all-fiber FFLs. For zero-bandgap graphene, the modulation depth is a bit low for mid-IR pulsed fiber lasers. A TI such as Bi_2Te_3 has a gapless surface state and a bulk bandgap of 0.35 eV [32]; however, the indirect bulk bandgap and complicated preparation process hinder its application as a mid-IR SA. A TMD such as MoS_2 generally has a large bandgap. Although the bandgap of MoS_2 can be reduced to 0.08 eV by introducing an atomic defect [33], no mode-locking operation has been reported with MoS_2 at 2.8 μm. Compared to other 2D SAs, BP is more suitable as a mid-IR SA for pulsed FFLs due to its layer-dependent direct bandgap and moderate modulation depth [34]. Combined with a gold-coated mirror, BP has been successfully used in mid-IR *Q*-switched and mode-locked Er:ZBLAN lasers at 2.8 μm and 3.5 μm wavelengths [35–37].

In this work, we report, to the best of our knowledge, the first pulsed all-fiber FFL in the mid-IR region. With a mechanically exfoliated BP flake as the SA, stable *Q*-switched

and mode-locked pulses were obtained from a robust and compact Er:ZBLAN fiber laser. In the *Q*-switching regime, the laser delivered an average power of 18.6 mW with a pulse duration of 3.4 μs and a repetition rate of 21.9 kHz at 2771.5 nm. For CW mode-locking operation, picosecond pulses with an average power of 6.2 mW and a repetition rate of 27.4 MHz were obtained at the wavelength of 2771.1 nm.

2. EXPERIMENTAL SETUP

Figure 1 shows the experimental setup of a pulsed all-fiber Er:ZBLAN laser incorporated with a BP SA. The pump source is a commercial 976 nm laser diode with a pigtail silica fiber, having a numerical aperture (NA) of 0.22 and core diameter of 105 μm. Its fiber end facet was coated with dielectric film before inserting it into a fiber connector (SMA905), having a transmission of 92% at 976 nm and a reflectivity of ~99.5% from 2400 nm to 2900 nm. Both the coated silica fiber and uncoated fluoride fiber were inserted into fiber connectors and fixed with glue (NOA61). We carefully inserted the fibers into fiber connectors by monitoring the transmitting pump beam shape and power, which may avoid the damage of perpendicularly cleaved fiber faces. In order to connect the pump fiber to the gain fiber, two fiber connectors were butted against each other and fixed by an adapter, as shown in Fig. 1 (upper). The inner image of the fiber connectors is presented in Fig. 1 (lower), in which much more detailed fiber parameters and laser structure are given. From the inner image, we could see that the pump light, delivered from the coated silica fiber with an NA of 0.22 and a core diameter of 105 μm, could be easily butt-coupled into the cladding of the fluoride gain fiber due to its larger NA (0.51) and larger diameter (251 μm). The ~3.7 m long double-clad 6 mol.% Er:ZBLAN fiber (FiberLabs Inc.) had a core diameter of 19.4 μm and core NA of 0.1. At the end of the gain fiber, a perpendicularly cleaved fiber tip was inserted into the fiber connector and fixed by glue. The high-refractive-index glue also worked as a clad-mode stripper (CMS) to remove the residual pump light, which might destroy the BP SA. The inset in Fig. 1 shows a photograph of the

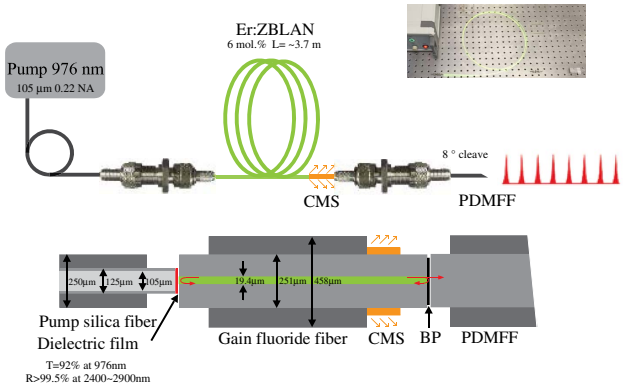

Fig. 1. Experimental setup of the pulsed all-fiber Er:ZBLAN laser (upper) and inner image of the fiber connectors (lower). BP, black phosphorus; CMS, clad-mode stripper; PDMFF, power-delivering multimode fluoride fiber. The inset shows a photograph of the pulsed all-fiber Er:ZBLAN laser.

compact and simple all-pulsed FFL based on a BP SA at 2.8 μm.

With the mechanical exfoliation method, we fabricated a BP flake with the size of 1 mm and thickness of about 100 nm. Compared to the liquid phase exfoliation method, the mechanical exfoliation method is more beneficial to obtain large-sized and high-quality 2D materials. The detailed fabrication process has been reported in previous work [24]. The exfoliated BP flake was adhered onto the fluoride fiber end facet, totally covering the core area of the gain fiber. Then, the BP flake was sandwiched between the fluoride gain fiber and power-delivering multimode fluoride fiber (PDMFF), and fixed by a fiber adapter. Its morphology and nonlinear optical absorption have been characterized in our previous work, showing a modulation depth of 19% and a saturable fluence of 9 $\mu J/cm^2$ [36]. The laser via Fresnel reflection between BP flake and PDMFF was modulated by the BP SA, resulting in *Q*-switched pulse generation. As we all know, BP tends to be oxidized, and fluoride glass tends to degenerate in the atmosphere. Both BP and fluoride fiber facets can be protected by sealing the fiber adapter with glue. The all-fiber cavity design can effectively improve mechanical and chemical stability. In order to avoid parasitic oscillation, the fiber end facet of the PDMFF was cleaved with an angle of 8°.

3. *Q*-SWITCHED Er:ZBLAN FIBER LASER

The bulk BP, provided by a commercial supplier (XFNANO Ltd.), was exfoliated mechanically into a 2D integratable flake. The mechanical-exfoliated BP flake has been demonstrated to possess a saturable absorption property at 2.8 μm in our previous work [36]. Without BP SA, the Er:ZBLAN fiber laser worked in a CW regime. After the transmission-type BP SA was integrated into the Er:ZBLAN fiber laser, the *Q*-switched pulses could be obtained from 511 mW to 796 mW of the launched pump power. At the launched pump power of 796 mW, the typical *Q*-switched pulse train was recorded at 22.41 kHz with a mid-IR photoelectric detector (Vigo System PCI-9), as shown in Fig. 2(a). The stability of the pulse train was measured by a radio frequency (RF) spectrum analyzer. The RF spectrum shows a signal-to-noise ratio (SNR) of 30 dB in Fig. 2(b). Figure 2(c) shows the *Q*-switched pulse profile with a pulse duration of 3.42 μs.

Figure 3 presents the laser performance evolution of the BP *Q*-switched all-fiber Er:ZBLAN laser with the launched pump power. When the launched pump power increased from 511 mW to 796 mW, the average power increased from 2.3 mW to 18.4 mW, and the pulse energy increased from 0.29 μJ to 0.82 μJ, as seen in Fig. 3(a). As expected, the pulse repetition rate increased, and the pulse duration decreased. The shortest pulse duration of 3.32 μs was obtained at the repetition rate of 22.2 kHz. When the launched pump power was beyond 796 mW, average power and pulse energy tended to saturate. BP is oxidized upon exposure to air. The oxidization process takes place only on the surface and tends to saturate after a few days [37,38]. With the surface-oxidized BP as the SA, the *Q*-switched pulses were stable in the long term. The *Q*-switched laser can serve as a mid-IR microsecond seed source for power scaling.

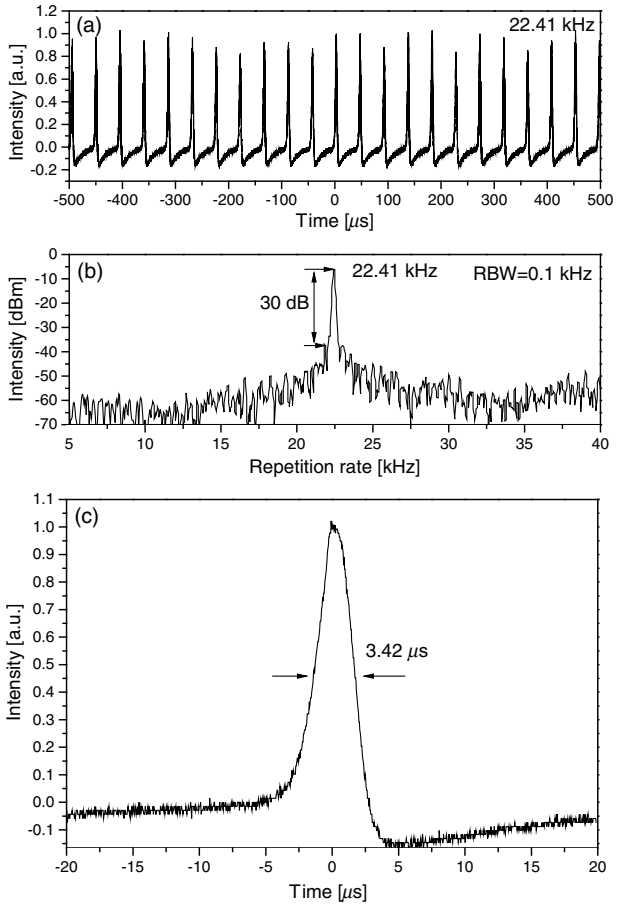

Fig. 2. (a) Typical *Q*-switched pulse train in 1 ms time scale. (b) RF spectrum with an SNR of 30 dB measured by a resolution bandwidth (RBW) of 0.1 kHz. (c) *Q*-switched pulse profile with a pulse duration of 3.42 μs.

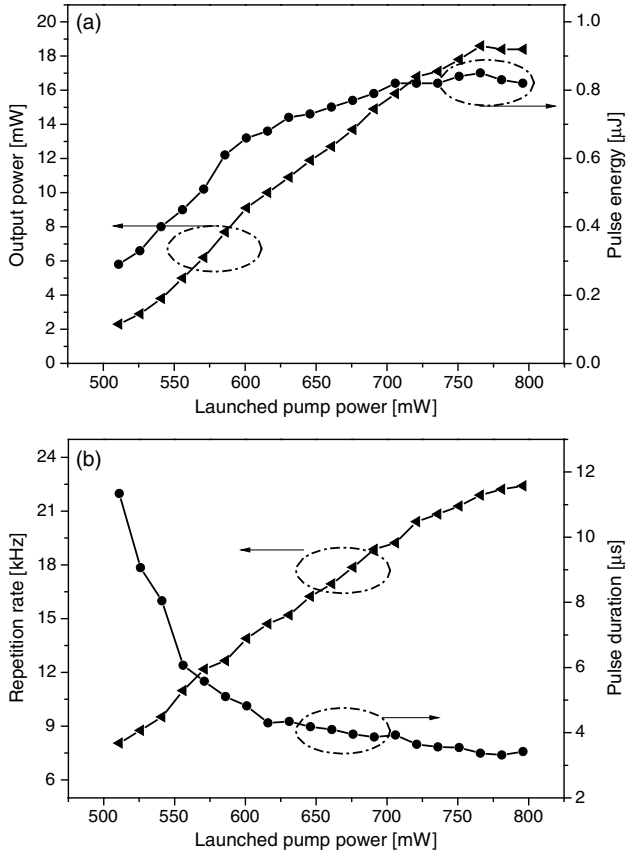

Fig. 3. (a) Average power and pulse energy versus the launched pump power. (b) Repetition rate and pulse duration versus the launched pump power.

Figure 4 shows the spectrum of a BP *Q*-switched all-fiber Er:ZBLAN laser. It was measured by a mid-IR optical spectrum analyzer with a resolution of 0.22 nm (Ocean Optics, SIR5000). The *Q*-switched spectrum centered at 2771.5 nm with a full width at half maximum (FWHM) of 1.5 nm. It is well known that water vapor absorption lines overlap with the amplified spontaneous emission spectrum of Er:ZBLAN in the range of 2.7–2.8 μm [39]. The effect of water vapor absorption can be eliminated based on the all-fiber cavity structure.

4. MODE-LOCKED Er:ZBLAN FIBER LASER

In the BP *Q*-switched Er:ZBLAN fiber laser, the reflectivity of the output coupler is too low to initiate a mode-locking operation. In order to improve the intracavity power, the PDMFF can be replaced by a dielectric mirror (DM) or coated with high-reflectivity dielectric film. Here we chose a coated DM with a reflectivity of 90% at 2800 nm due to the current immature coating process on a fluoride fiber facet. At a launched pump power of 796 mW, we observed the typical *Q*-switched mode-locking operation, as shown in Fig. 5(a). The mode-locked pulse train was intensity modulated at a repetition rate of 22.8 kHz. The intensity modulation profile had a time duration of 8 μs. The repetition rate of the

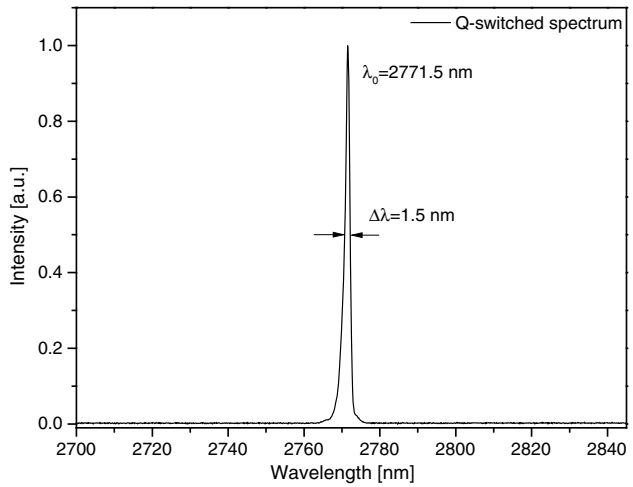

Fig. 4. BP *Q*-switched spectrum of all-fiber Er:ZBLAN laser.

Q-switching profile increased with the launched pump power. At the launched pump power of 900 mW, the repetition rate of the *Q*-switching profile increased to 31.3 kHz [Fig. 5(b)]. In the microsecond time scale, the pulse train showed mode-locked pulses with an interval of 36.5 ns, corresponding to a repetition rate of 27.4 MHz, as shown in Fig. 5(c).

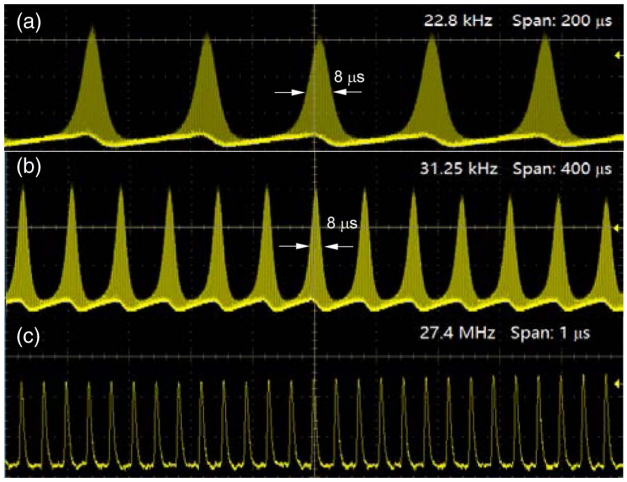

Fig. 5. (a) *Q*-switched mode-locked pulse train at 796 mW of launched pump power in the 200 μs time scale, (b) *Q*-switched mode-locked pulse train at 900 mW of launched pump power in the 400 μs time scale, and (c) *Q*-switched mode-locked pulse train at 796 mW of launched pump power in the 1 μs time scale.

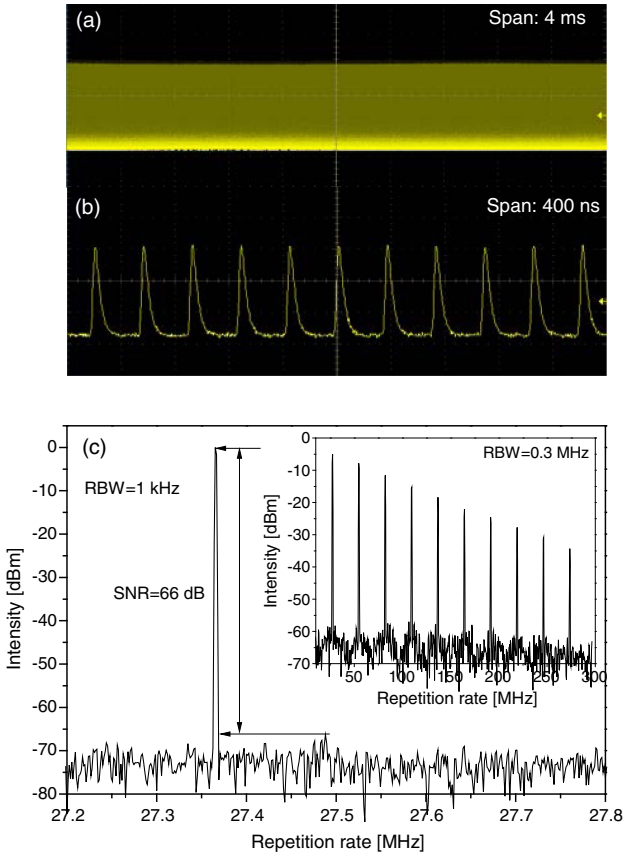

Fig. 6. (a) CW mode-locked pulse train in the millisecond time scale and (b) CW mode-locked pulse train in the nanosecond time scale. (c) Fundamental RF spectrum with an SNR of 66 dB measured by an RBW of 1 kHz. The inset is a broader RF spectrum measured by an RBW of 0.3 MHz.

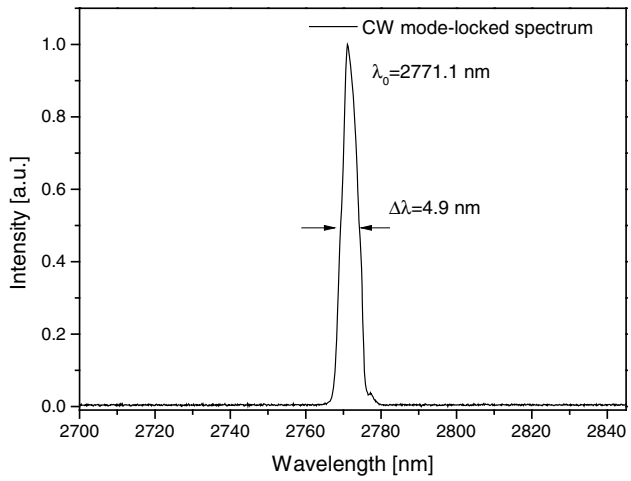

Fig. 7. CW mode-locked pulse spectrum.

By further increasing the launched pump power up to 1050 mW, CW mode-locking operation was achieved with an average power of 6.2 mW and could be sustained in the long term. In the millisecond time scale [Fig. 6(a)], the pulse intensity is uniform without any *Q*-switching instability. The mode-locked pulse train in Fig. 6(b) shows a pulse period of 36.5 ns, which is inconsistent with the round-trip time of a pulse in the cavity. Using the RF analyzer, we recorded a fundamental beat signal at 27.4 MHz with an SNR of 66 dB [Fig. 6(c)], indicating very stable mode locking. A broader RF spectrum [inset of Fig. 6(c)] was analyzed, and only harmonic beats were observed. The Er:ZBLAN fiber laser operated in a fundamental transverse mode.

In the mode-locking regime, the low average output power was attributed to the low output coupling and possible BP damage under high pump power. Limited by the low sensitivity of a commercial autocorrelator at 2.8 μm and low average power of the laser, we failed to achieve the pulse duration by a commercial autocorrelator (APE PulseCheck USB 150 MIR). The pulse duration was estimated to be tens of picoseconds according to previous results, where a mode-locked Er:ZBLAN laser was demonstrated with the mechanically exfoliated BP SA [36]. Figure 7 shows the CW mode-locked spectrum. Compared to the *Q*-switched spectrum, the spectral bandwidth was obviously broadened from 1.5 nm to 4.9 nm.

5. CONCLUSION

In conclusion, we demonstrated the all-fiber *Q*-switched and mode-locked FFLs by using an integratable BP SA and two pairs of fiber connectors. The integration of BP reduced the use of fiber optic devices, enabling the realization of an all-fiber laser. Compared to previous *Q*-switched and mode-locked FFLs incorporated with numerous free-space optic elements, here, the pulsed all-fiber FFL is more stable and compact. To the best of our knowledge, this is the first time a pulsed all-fiber FFL has been achieved in the mid-IR region. We believe that this is the beginning for exploring all-fiber mid-IR ultrafast laser sources. With the increasing demand for mid-IR coherent sources, the development of an all-fiber mid-IR pulsed laser will become more and more important due to its stability and compactness.

Funding. National Basic Research Program of China (2013CBA01505); National Natural Science Foundation of China (NSFC) (11721091, 61675130); National Postdoctoral Program for Innovative Talents (BX20170149); China Postdoctoral Science Foundation (2017M620150).

REFERENCES

1. B. G. Lee, M. A. Belkin, R. Audet, J. MacArthur, L. Diehl, C. Pflügl, F. Capasso, D. C. Oakley, D. Chapman, A. Napoleone, D. Bour, S. Corzine, G. Höfler, and J. Faist, "Widely tunable single-mode quantum cascade laser source for mid-infrared spectroscopy," Appl. Phys. Lett. **91**, 231101 (2007).
2. H. H. P. T. Bekman, J. C. van den Heuvel, F. J. M. van Putten, and H. M. A. Schleijpen, "Development of a mid-infrared laser for study of infrared countermeasures techniques," Proc. SPIE **5615**, 27–38 (2004).
3. D. Halmer, S. Thelen, P. Hering, and M. Mürtz, "Online monitoring of ethane traces in exhaled breath with a difference frequency generation spectrometer," Appl. Phys. B **85**, 437–443 (2006).
4. C. R. Petersen, N. Prtljaga, M. Farries, J. Ward, B. Napier, G. R. Lloyd, J. Nallala, N. Stone, and O. Bang, "Mid-infrared multispectral tissue imaging using a chalcogenide fiber supercontinuum source," Opt. Lett. **43**, 999–1002 (2018).
5. Y. O. Aydin, V. Fortin, F. Maes, F. Jobin, S. D. Jackson, R. Vallée, and M. Bernier, "Diode-pumped mid-infrared fiber laser with 50% slope efficiency," Optica **4**, 235–238 (2017).
6. O. Henderson-Sapir, J. Munch, and D. J. Ottaway, "Mid-infrared fiber lasers at and beyond 3.5 μm using dual-wavelength pumping," Opt. Lett. **39**, 493–496 (2014).
7. O. Henderson-Sapir, J. Munch, and D. J. Ottaway, "New energy-transfer upconversion process in Er^{3+}:ZBLAN mid-infrared fiber lasers," Opt. Express **24**, 6869–6883 (2016).
8. F. Maes, V. Fortin, M. Bernier, and R. Vallée, "Quenching of 3.4 μm dual-wavelength pumped erbium doped fiber lasers," IEEE J. Quantum Electron. **53**, 1600208 (2017).
9. M. Heck, S. Nolte, A. Tünnermann, R. Vallée, and M. Bernier, "Femtosecond-written long-period gratings in fluoride lasers," Opt. Lett. **43**, 1994–1997 (2018).
10. V. Fortin, M. Bernier, S. T. Bah, and R. Vallée, "30 W fluoride glass all-fiber laser at 2.94 μm," Opt. Lett. **40**, 2882–2885 (2015).
11. F. Maes, V. Fortin, M. Bernier, and R. Vallée, "5.6 W monolithic fiber laser at 3.55 μm," Opt. Lett. **42**, 2054–2057 (2017).
12. Z. Qin, G. Xie, J. Ma, P. Yuan, and L. Qian, "Mid-infrared Er:ZBLAN fiber laser reaching 3.68 μm wavelength," Chin. Opt. Lett. **15**, 111402 (2017).
13. C. A. Schafer, H. Uehara, D. Konishi, S. Hattori, H. Matsukuma, M. Murakami, S. Shimizu, and S. Tokita, "Fluoride-fiber-based side-pump coupler for high-power fiber lasers at 2.8 μm," Opt. Lett. **43**, 2340–2343 (2018).
14. Z. Zheng, D. Ouyang, J. Zhao, M. Liu, S. Ruan, P. Yan, and J. Wang, "Scaling all-fiber mid-infrared supercontinuum up to 10 W-level based on thermal-spliced silica fiber and ZBLAN fiber," Photon. Res. **4**, 135–139 (2016).
15. J. Ma, G. Q. Xie, P. Lv, W. L. Gao, P. Yuan, L. J. Qian, H. H. Yu, H. J. Zhang, J. Y. Wang, and D. Y. Tang, "Graphene mode-locked femtosecond laser at 2 μm wavelength," Opt. Lett. **37**, 2085–2087 (2012).
16. G. Q. Xie, J. Ma, P. Lv, W. L. Gao, P. Yuan, L. J. Qian, H. H. Yu, H. J. Zhang, J. Y. Wang, and D. Y. Tang, "Graphene saturable absorber for *Q*-switching and mode-locking at 2 μm wavelength [Invited]," Opt. Mater. Express **2**, 878–883 (2012).
17. G. Sobon, "Mode-locking of fiber lasers using novel two-dimensional nanomaterials: graphene and topological insulators [Invited]," Photon. Res. **3**, A56–A63 (2015).
18. L. C. Kong, G. Q. Xie, P. Yuan, L. J. Qian, S. X. Wang, H. H. Yu, and H. J. Zhang, "Passive *Q*-switching and *Q*-switched mode-locking operations of 2 μm Tm:CLNGG laser with MoS_2 saturable absorber mirror," Photon. Res. **3**, A47–A50 (2015).
19. C. Zhu, F. Wang, Y. Meng, X. Yuan, F. Xiu, H. Luo, Y. Wang, J. Li, X. Lv, L. He, Y. Xu, J. Liu, C. Zhang, Y. Shi, R. Zhang, and S. Zhu, "A robust and tuneable mid-infrared optical switch enabled by bulk Dirac fermions," Nat. Commun. **8**, 14111 (2017).
20. Y. F. Song, L. Li, H. Zhang, D. Y. Shen, D. Y. Tang, and K. P. Loh, "Vector multi-soliton operation and interaction in a graphene mode-locked fiber laser," Opt. Express **21**, 10010–10018 (2013).
21. Y. F. Song, H. Zhang, L. M. Zhao, D. Y. Shen, and D. Y. Tang, "Coexistence and interaction of vector and bound vector solitons in a dispersion-managed fiber laser mode locked by graphene," Opt. Express **24**, 1814–1822 (2016).
22. G. Zhu, X. Zhu, F. Wang, S. Xu, Y. Li, X. Guo, K. Balakrishnan, R. A. Norwood, and N. Peyghambarian, "Graphene mode-locked fiber laser at 2.8 μm," IEEE Photon. Technol. Lett. **28**, 7–10 (2016).
23. L. Kong, Z. Qin, G. Xie, Z. Guo, H. Zhang, P. Yuan, and L. Qian, "Black phosphorus as broadband saturable absorber for pulsed lasers from 1 μm to 2.7 μm wavelength," Laser Phys. Lett. **13**, 045801 (2016).
24. Y. Chen, G. Jiang, S. Chen, Z. Guo, X. Yu, C. Zhao, H. Zhang, Q. Bao, S. Wen, D. Tang, and D. Fan, "Mechanically exfoliated black phosphorus as a new saturable absorber for both *Q*-switching and mode-locking operation," Opt. Express **23**, 12823–12833 (2015).
25. S. B. Lu, L. L. Miao, Z. N. Guo, X. Qi, C. J. Zhao, H. Zhang, S. C. Wen, D. Y. Tang, and D. Y. Fan, "Broadband nonlinear optical response in multilayer black phosphorus: an emerging infrared and mid-infrared optical material," Opt. Express **23**, 11183–11194 (2015).
26. Z. C. Luo, M. Liu, Z. N. Guo, X. F. Jiang, A. P. Luo, C. J. Zhao, X. F. Yu, W. C. Xu, and H. Zhang, "Microfiber-based few-layer black phosphorus saturable absorber for ultra-fast fiber laser," Opt. Express **23**, 20030–20039 (2015).
27. H. Mu, S. Lin, Z. Wang, S. Xiao, P. Li, Y. Chen, H. Zhang, H. Bao, S. P. Lau, C. Pan, D. Fan, and Q. Bao, "Black phosphorus-polymer composites for pulsed lasers," Adv. Opt. Mater. **3**, 1447–1453 (2015).
28. D. Li, H. Jussila, L. Karvonen, G. Ye, H. Lipsanen, X. Chen, and Z. Sun, "Polarization and thickness dependent absorption properties of black phosphorus: new saturable absorber for ultrafast pulse generation," Sci. Rep. **5**, 15899 (2015).
29. J. Ma, S. Lu, Z. Guo, X. Xu, H. Zhang, D. Tang, and D. Fan, "Few-layer black phosphorus based saturable absorber mirror for pulsed solid-state lasers," Opt. Express **23**, 22643–22648 (2015).
30. Y. Song, S. Chen, Q. Zhang, L. Li, L. Zhao, H. Zhang, and D. Tang, "Vector soliton fiber laser passively mode locked by few layer black phosphorus-based optical saturable absorber," Opt. Express **24**, 25933–25942 (2016).
31. C. Wei, H. Luo, H. Zhang, C. Li, J. Xie, J. Li, and Y. Liu, "Passively *Q*-switched mid-infrared fluoride fiber laser around 3 μm using a tungsten disulfide (WS_2) saturable absorber," Laser Phys. Lett. **13**, 105108 (2016).
32. Y. L. Chen, J. G. Analytis, J.-H. Chu, Z. K. Liu, S.-K. Mo, X. L. Qi, H. J. Zhang, D. H. Lu, X. Dai, Z. Fang, S. C. Zhang, I. R. Fisher, Z. Hussain, and Z.-X. Shen, "Experimental realization of a three-dimensional topological insulator, Bi_2Te_3," Science **325**, 178–181 (2009).
33. S. Wang, H. Yu, H. Zhang, A. Wang, M. Zhao, Y. Chen, L. Mei, and J. Wang, "Broadband few-layer MoS_2 saturable absorbers," Adv. Mater. **26**, 3538–3544 (2014).
34. V. Tran, R. Soklaski, Y. Liang, and L. Yang, "Layer-controlled band gap and anisotropic excitons in few-layer black phosphorus," Phys. Rev. B **89**, 235319 (2014).
35. Z. Qin, G. Xie, H. Zhang, C. Zhao, P. Yuan, S. Wen, and L. Qian, "Black phosphorus as saturable absorber for the *Q*-switched Er:ZBLAN fiber laser at 2.8 μm," Opt. Express **23**, 24713–24718 (2015).
36. Z. Qin, G. Xie, C. Zhao, S. Wen, P. Yuan, and L. Qian, "Mid-infrared mode-locked pulse generation with multilayer black phosphorus as saturable absorber," Opt. Lett. **41**, 56–59 (2016).
37. Z. Qin, T. Hai, G. Xie, J. Ma, P. Yuan, L. Qian, L. Li, L. Zhao, and D. Shen, "Black phosphorus *Q*-switched and mode-locked mid-infrared Er:ZBLAN fiber laser at 3.5 μm wavelength," Opt. Express **26**, 8224–8231 (2018).
38. M. T. Edmonds, A. Tadich, A. Carvalho, A. Ziletti, K. M. O'Donnell, S. P. Koenig, D. F. Coker, B. Özyilmaz, A. H. Neto, and M. S. Fuhrer, "Creating a stable oxide at the surface of black phosphorus," ACS Appl. Mater. Interfaces **7**, 14557–14562 (2015).
39. S. Antipov, D. D. Hudson, A. Fuerbach, and S. D. Jackson, "High-power mid-infrared femtosecond fiber laser in the water vapor transmission window," Optica **3**, 1373–1376 (2016).